Journal of Power Sources 180 (2008) 852–858

Contents lists available at ScienceDirect

Journal of Power Sources

journal homepage: www.elsevier.com/locate/jpowsour

PMMA-assisted synthesis of $Li_{1-x}Ni_{0.5}Mn_{1.5}O_{4-\delta}$ for high-voltage lithium batteries with expanded rate capability at high cycling temperatures

J.C. Arrebola, A. Caballero, L. Hernán*, J. Morales

Departamento de Química Inorgánica e Ingeniería Química, Campus de Rabanales, Edificio Marie Curie, Universidad de Córdoba, 14071 Córdoba, Spain

ARTICLE INFO

Article history:
Received 4 December 2007
Received in revised form 30 January 2008
Accepted 17 February 2008
Available online 2 March 2008

Keywords:
PMMA
Spinel
Lithium batteries
High temperature

ABSTRACT

In this work, poly(methyl methacrylate) (PMMA), a non-surfactant polymer was used to synthesize non-stoichiometric $Li_{0.82}Ni_{0.52}Mn_{1.52}O_{4-\delta}$ ($0 \le \delta \le 0.25$) spinels. The presence of the polymer was found to be beneficial with a view to facilitating the use of the spinel in electrodes for lithium batteries. Thus, PMMA allowed spinel particles of a high crystallinity and uniform size and shape to be obtained, and particle size to be tailored by using an appropriate calcining temperature and time. By controlling these variables, spinels in nanometric, submicrometric and micrometric particle sizes were prepared and characterized by chemical analysis, X-ray diffraction, electron microscopy, thermogravimetry and nitrogen adsorptions measurements. The spinels were obtained as highly crystalline phases with lithium and oxygen deficiency and some cation disorder as revealed by chemical analysis, thermogravimetric and XRD data. Their electrochemical performance in two-electrode cells was tested at room temperature and 50 °C over a wide range of charge/discharge rates (from *C*/4 to 4*C*). Cell performance was found to depend on particle size rather than on structural properties. Thus, the spinel best performing at 50 °C was that consisting of submicrometric particles, which delivered a high capacity and exhibited the best capacity retention and rate capability. Particles of submicronic size share the advantages of nanometric particles (*viz.* the ability to withstand high charge/discharge rates) and micrometric particles (a high capacity and stability at low rates).

1. Introduction

The study of inorganic materials amenable to use as electrodes in lithium batteries is by now a consolidated research area by virtue of the technological significance of these electrochemical storage energy devices [1,2]. The underlying electrochemical reaction is mainly governed by the electrode/electrolyte interface, so accurately controlling particle surface properties is essential with a view to ensuring good cell performance. Polymer-assisted synthesis is a novel method for tailoring particle shape and size in transition metal oxides [3–5], many of which are used as electrode materials in lithium cells. In this context, we recently reported the use of a surfactant polymer, polyethylene glycol-400, in the synthesis of $LiNi_{0.5}Mn_{1.5}O_4$ spinel [6], which is the most attractive choice for a new generation of lithium-ion batteries with higher voltages than those based on $LiCoO_2$ system currently available [7]. The material was obtained as highly crystalline nanoparticles exhibiting very good performance upon cycling at ambient temperature over a wide range of charge/discharge rates (from *C*/4 to 15*C*). At higher temperatures, which may be common working conditions in future applications such as hybrid vehicles, however, their performance was only acceptable at high charge/discharge rates. This may be a result of side reactions related with the electrolyte decomposition [8] (e.g. $LiPF_6 + H_2O \rightarrow POF_3 + LiF + 2HF$) detracting from performance under these conditions. The $LiMn_2O_4$ spinel has been found to be especially sensitive to this reaction [9], since the HF released may attack Mn^{3+} sites and cause its partial dissolution, thereby impairing cell performance. Although the spinel $LiNi_{0.5}Mn_{1.5}O_4$ formally lacks Mn^{3+}, the presence of some Ni^{3+}, as revealed by XPS [10,11] may invalidate this stoichiometric assumption and account for its vulnerability to attack by the electrolyte decomposition products.

At high rates, where the electrode/electrolyte contact time is short, the decomposition reaction occurs to a negligible extent and the cell retains its good performance. At low rates, the conditions are reversed and the decomposition reaction is quite favorable, as revealed by cyclic voltammetric data [12]. Thus, nanometric spinel particles can be partially dissolved by HF released in the reaction and the lithium insertion/extraction process be deteriorated. One widely used method to circumvent this shortcoming involves coating the active particles with a material easily reacting with HF such as ZnO [13]. This remedy proved effective – a $LiNi_{0.5}Mn_{1.5}O_4$ spinel

* Corresponding author. Fax: +34 957 218621.
E-mail address: iq1hepal@uco.es (L. Hernán).

0378-7753/$ – see front matter © 2008 Elsevier B.V. All rights reserved.
doi:10.1016/j.jpowsour.2008.02.076

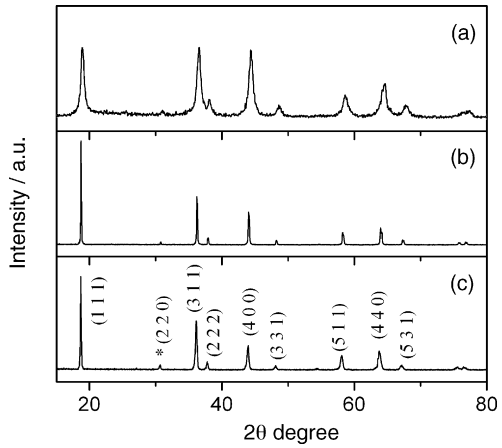

Fig. 1. XRD patterns for (a) the precursor calcined at 400 °C, (b) S-800-5 and (c) S-900-48.

prepared as micrometric particles exhibited substantially improved cyclability when coated with nanosized ZnO – but measurements were performed at a low rate (*C*/3). The coating methodology, however, deteriorates the surface of the active particles as the coating is carried out in a liquid suspension. This can raise the surface impedance and degrade the rate capability of the material as a result. This was experimentally confirmed by Chen and Dahn [14] in Al_2O_3-coated $LiCoO_2$. In order to avoid this problem, we used an alternative method involving deposition of the coater from a gas phase [15]. The coater was a layer of gold, a noble metal which is stable towards reactive compounds such as HF and should therefore protect particles against the dissolving activity of the electrolyte while raising the electronic conductivity of the electrode. However, even this clean, soft method failed to improve cell performance at high rates because the coating layer formed a barrier that was difficult to cross by the lithium ions.

In this work, we developed an alternative method for improving the rate capability based on accurate control of particle size (in between nanometric and micrometric size) since a small particle size affords high charge discharge rates (above 1*C*), whereas a large size results good performance at lower rates. An appropriate selection of the synthesis method is crucial with a view to succeeding here. As stated above, the use of polymers is now a common choice for controlling particle growth. In fact, polymers can encapsulate particles, growth of which is governed by the heating temperature and time. Poly(methyl methacrylate), PMMA [16,17], yielded the best results among the polymers studied. Grinding the precursors prior to removing the polymer by thermal decomposition was found to provide more homogeneous materials. By using a controlled heating temperature and time, highly pure Li–Ni–Mn–O spinel with average particle size ranging from 40 nm to 5 μm was obtained the electrochemical properties of which in lithium cells at 50 °C were quite good over a wide range of charge/discharge rates provided the particles were submicronic in size.

One advantage of the spinel structure is the three dimensional network of holes available for ion mobility. The mechanism proposed for ion displacement in such a network involves traveling through a 8a → 16c → 8a → 16c → diffusion path [18]. Therefore, the presence of vacancies at 8a positions may be beneficial with a view to improving the kinetics of Li extraction and insertion. We considered this factor in the synthesis of the spinels, which were thus prepared with a slight Li deficiency. Nonstoichiometric Li–Mn–O-based spinels have been found to exhibit capacity retention at elevated temperatures [19].

2. Experimental

Samples were obtained from mixtures of $MnAc_2{\cdot}4H_2O$, $NiAc_2{\cdot}4H_2O$ and $LiAc{\cdot}1/3H_2O$ (Ac = CH_3–COO^-) in 1:0.5:0.85 mol proportion with $H_2C_2O_4{\cdot}2H_2O$ [20]. In a typical synthetic run, 5 g of

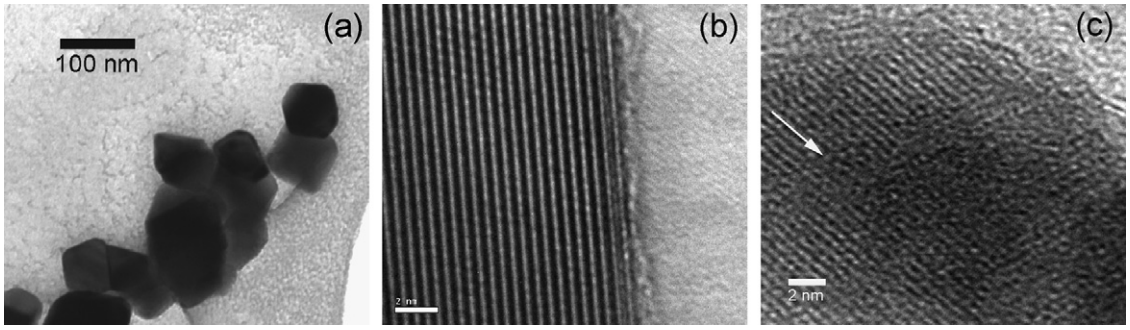

Fig. 2. (a and b) TEM images of spinel S-800-0 and (c) TEM image of the precursor heated at 400 °C.

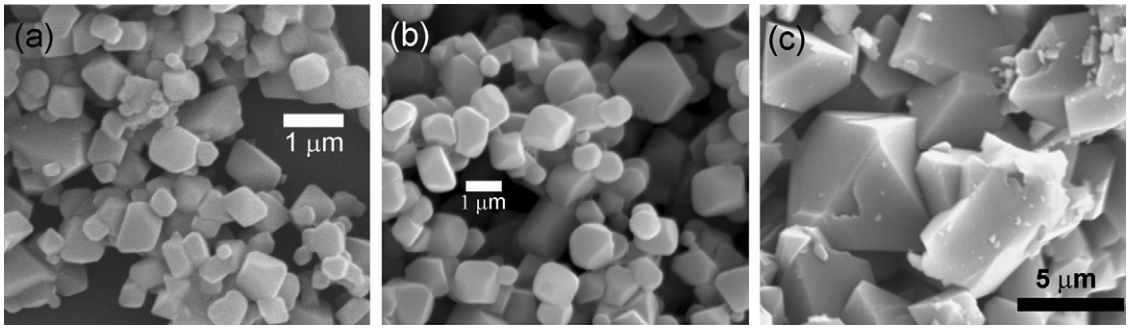

Fig. 3. SEM images of spinels (a) S-800-5, (b) S-800-24 and (c) S-900-48.

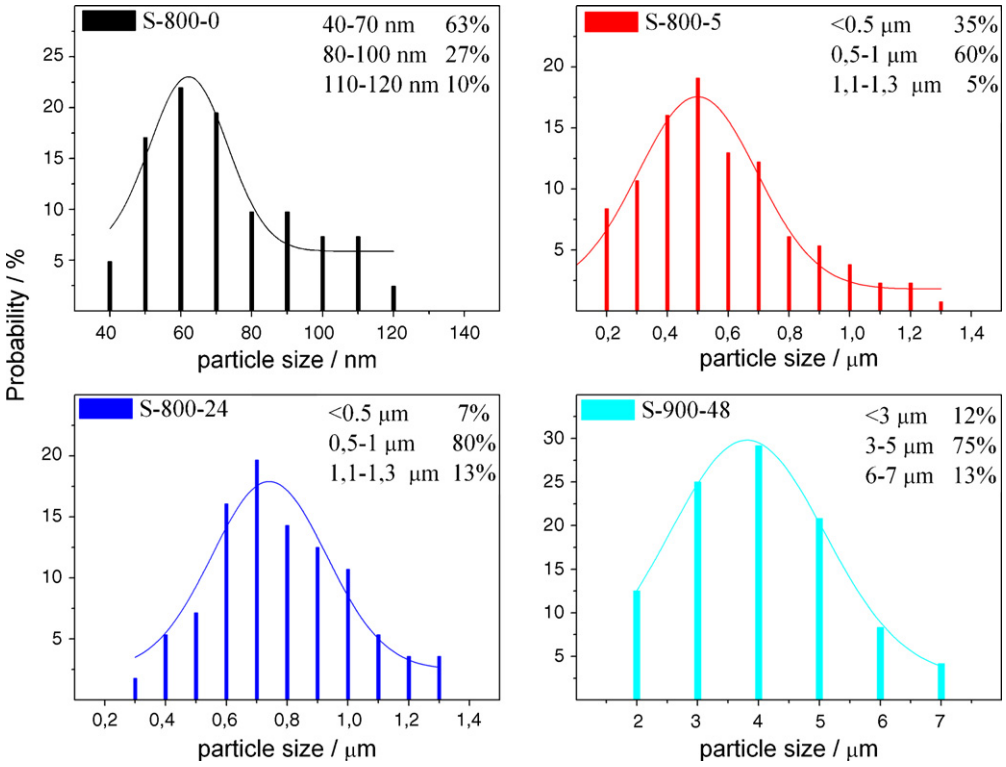

Fig. 4. Particle size distribution histogram obtained from the TEM and SEM images for samples (a) S-800-0, (b) S-800-5, (c) S-800-24 and (d) S-900-48.

mixed precursor and 2.5 g of oxalic acid were ground to a homogeneous mixture in a planetary Restach ball mill at 60 rpm for 3 min, using agate balls and an agate jar. In a second step, 2.5 g of PMMA was added and grinding continued for another 60 min to ensure thorough mixing of the chemicals and polymer. The product thus obtained was a green solid which was calcined at 400 °C for 12 h and then up to 800 °C at a heating rate of 15 °C min^{-1}, followed by switching off the furnace to obtain the spinel. The resulting sample was named S-800-0 and used to prepare the other samples simply by calcining again at 800 °C for 5 (sample S-800-5) or 24 h (sample S-800-24). One other sample (S-900-48) was prepared by raising the temperature at 900 °C and heating for 48 h. The chemical composition was determined by induced couple plasma analysis on a Fisons ARL-3410 instrument.

XRD patterns were recorded on a Siemens D5000 X-ray diffractometer using non-monochromated Cu Kα radiation and a graphite monochromator for the diffracted beam. The scanning conditions for structural refinement were 15–90° (2θ), a 0.03° step size and 12 s per step. Transmission electron microscopy (TEM) images were obtained with a Phillips TEM instrument operating at 100 keV and SEM images with a Jeol 6400 scanning electron microscope. Specific surface areas were determined with a Micromeritics ASAP 2010 instrument using N_2 gas as adsorbate.

Electrochemical measurements were made on CR2032 coin-type cells supplied by Hohsen. Lithium metal (supplied by Strem) was used as anode and isolated from the cathode by means of a porous propylene film. The electrolyte, supplied by Merck, was 1 M anhydrous $LiPF_6$ in a 1:1 mixture of ethylene carbonate and dimethyl carbonate. Cells were assembled in an M-Braun glove-box. Step potential electrochemical spectroscopy (SPES) curves were recorded at 1.25 mV/20 s per step. Galvanostatic tests were conducted under different charge/discharge regimes (from *C*/4 to 8*C*, *C* representing 1 Li^+ ion exchanged in 1 h, equivalent to 148 mA g^{-1}). Both types of electrochemical measurements were controlled via a MacPile II potentiostat–galvanostat. All measurements were made at least in duplicate in order to ensure reliability in the electrochemical tests.

3. Results and discussion

3.1. Structural and morphological properties

On heating, the polymer was lost at quite low temperatures (below 400 °C). However, although all lines in the XRD pattern, Fig. 1a, obtained at 400 °C were fitted to the spinel structure, they were weak and broad, which is suggestive of a low crystallinity and hence of poor electrochemical performance [21]. In order to improve crystallinity, the calcining temperature was raised to 800 °C. Under these conditions, reflection peaks were stronger and sharper, a sign of improved crystallinity. No impurities such as NiO and/or Li_xNiO, which are frequently reported in the synthesis of this compound [22], were found; therefore, the proposed synthetic method yields a highly pure spinel. A preliminary inspection of the XRD patterns revealed an increase in unit cell dimension on prolonged heating and the presence of a weak peak at 31° 2θ which was assigned to the (2 2 0) reflection the presence of which suggests some contribution from the inverse spinel-type structure as discussed below. The unit cell value found for the S-800-0 sample is somewhat higher than those usually reported for stoichiometric $LiNi_{0.5}Mn_{1.5}O_4$ [23,24]. However, values similar to ours have also been reported [25,26]. On the other hand, the unusual values (*viz.* 8.220, 8.228 and 8.251 Å for the S-800-5, S-800-24 and S-900-48 spinels, respectively) may be due to an increased Mn^{3+} content the ionic radius of which is bigger than that of Mn^{4+}. If such is the case, then some oxygen must be released during the calcining process [27],

$$LiNi_{0.5}Mn_{1.5}O_4 \Rightarrow LiNi_{0.5}Mn_{1.5}O_{4-\delta} + \delta/2O_2 \quad (1)$$

and electroneutrality in the structure maintained as a result. In order to confirm this assumption, sample S-800-0 was calcined at

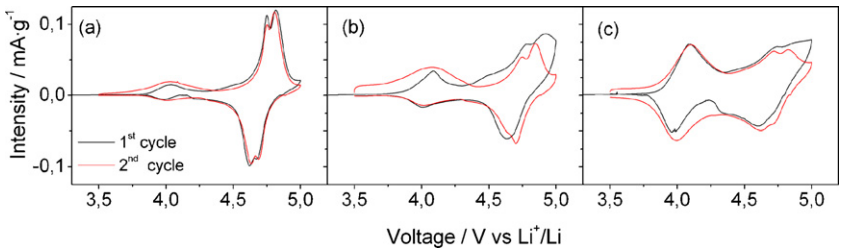

Fig. 5. SPES curves for (a) S-800-0, (b) S-800-5 and (c) S-900-48.

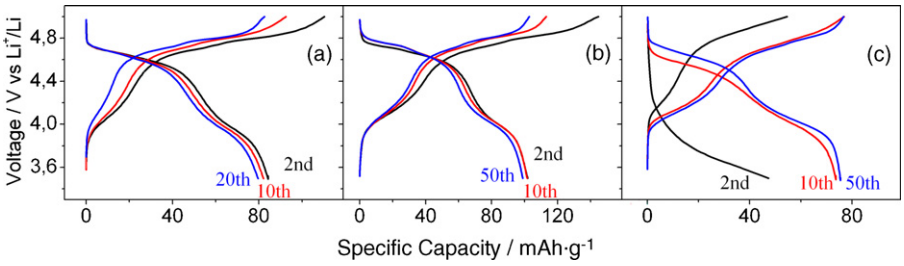

Fig. 6. Charge/discharge curves recorded at 25 °C at *C*/4 for samples (a) S-800-0, (b) S-800-5 and (c) S-900-48. The number of the cycles is shown.

Table 1
Formula, cation distribution, R_{wp}, lattice parameters, specific surface area ($m^2\ g^{-1}$) and crystallite size of the Li–Ni–Mn–O spinels

Sample	Formula (ICP)	Formula (weight loss)	Cation distribution (XRD)	R_{wp}	a (Å)	S_{BET}	D (nm)
S-800-0	$Li_{0.82}Ni_{0.52}Mn_{1.51}O_4$	$Li_{0.82}Ni_{0.52}Mn_{1.51}O_4$	$[Li_{0.81}Mn_{0.16}]_{8a}[Mn_{1.35}Ni_{0.52}]_{16d}O_4$	22.98	8.1961(5)	7.9(4)	65
S-800-5	$Li_{0.81}Ni_{0.54}Mn_{1.51}O_{3.90}$	$Li_{0.81}Ni_{0.54}Mn_{1.51}O_{3.85}$	$[Li_{0.8}Mn_{0.16}]_{8a}[Li_{0.03}Mn_{1.34}Ni_{0.54}]_{16d}O_{3.90}$	22.25	8.2217(9)	2.1(2)	469
S-900-48	$Li_{0.83}Ni_{0.52}Mn_{1.52}O_{3.87}$	$Li_{0.84}Ni_{0.52}Mn_{1.52}O_{3.72}$	$[Li_{0.7}Mn_{0.26}]_{8a}[Li_{0.14}Mn_{1.26}Ni_{0.52}]_{16d}O_{3.87}$	12.86	8.2506(8)	1.2(2)	–

800 °C for 5 and 24 h and at 900 for 48 h, and the resulting weight losses measured. The loss was 1.30, 1.32 and 2.50% for the first, second and third calcination, respectively. Therefore, prolonging the heating time at 800 °C from 5 to 24 h has little effect.

The results of the chemical analysis are shown in Table 1. Sample S-800-24 has been excluded owing to its similarity to S-800-5. The Mn/Ni ratios obtained were somewhat lower than the stoichiometric value of 3; however, the main difference from the stoichiometric spinel was that in the lithium content, which was *ca.* 0.82 atoms per formula. Also, a slight oxygen deficiency was observed in samples S-800-5 and S-900-48. These results are consistent with the trend in the oxygen content as derived from the weight loss data: the amount of oxygen released increased as the heating temperature was raised. However, the oxygen content found by chemical analysis was somewhat higher. The formulae obtained from the weight loss data and the metal contents obtained from the ICP analysis are also shown in Table 1.

Concerning cation distribution, the XRD patterns were subjected to Rietveld refinement by using the GSAS software [28]. As no peaks assignable to transition metal ordering were detected, data were fitted in the *Fd*3*m* space group. The most salient finding was a small fraction of transition metal ions occupying tetrahedral 8a sites, which is consistent with the presence of the (2 2 0) reflection as a weak peak. Based on the crystal field model, Ni^{2+} ions have a strong tendency to occupy octahedral positions (16d); therefore, Mn was forced to occupy tetrahedral positions (8a). One other interesting result was the evolution of the fraction of inverse spinel with heating. Thus, its content increased with increase in oxygen release and the Mn^{3+} content. On the other hand, the fitted curves were consistent with the presence of a slight oxygen deficiency in the spinel structural framework. Moreover, the cation deficiency tended to be canceled by the release of oxygen. The large unit cell values obtained for our spinels relative to the spinel of nominal composition $LiNi_{0.5}Mn_{1.5}O_4$ must have been a result of both the cation disorder and nonstoichiometry.

Fig. 2 shows TEM images of sample S-800-0; as can be seen, it consisted of particles rather uniform in size (average size *ca.* 60 nm) and exhibited the typical polyhedral shape of the spinel, which

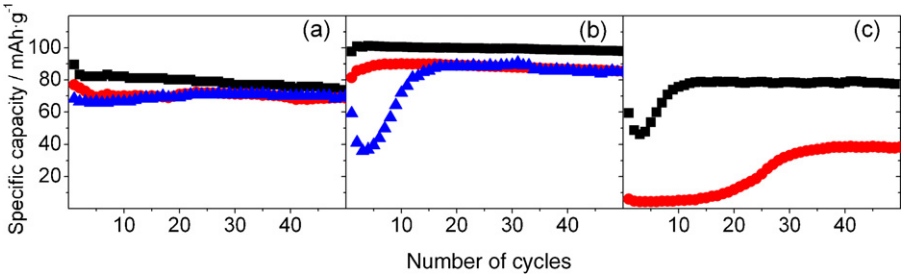

Fig. 7. Variation of specific capacity as a function of the number of cycles. Galvanostatic tests conducted at 25 °C. (a) S-800-0, (b) S-800-5 and (c) S-900-48. Rate: *C*/4 (black square); 2*C* (red circle); and 4*C* (blue triangle). (For interpretation of the references to color in this figure legend, the reader is referred to the web version of the article.)

reflects a high crystallinity. This is confirmed by the image of Fig. 2b, which was obtained at higher magnification. Fringes *ca.* 0.45 nm wide corresponding to the orientation of (1 1 1) atomic planes were well-ordered and aligned, and consistent with a low content in defects. An image of a particle heated at 400 °C obtained at the same magnification is shown in Fig. 2c for comparison. As stated above, the XRD pattern for this sample revealed a low crystallinity, consistent with increased disorder in the fringes and the presence of defects in such planes. Others authors [29] have obtained nanometric samples by using the polymer in various ways. The polymer creates a capping effect where the attractive Van der Waals forces between growing particles are suppressed, thereby limiting particle size. On heating at 800 °C for 5 h (sample S-800-5) particles increased in size; the SEM images of Fig. 3 are more illustrative of their overall morphology. As can be seen, the particles retained their polyhedral shape and well-defined faces, and increased in size by 0.5–1 μm. Prolonged heating (24 h) hardly affected particle size (Fig. 3b). Thus, obtaining larger particles entailed raising the heating temperature. Sample S-900-48, which was calcined at 900 °C for 48 h, consisted of micrometric particles around 5 μm in size (Fig. 3c). The specific surface areas obtained are listed in Table 1. As can be seen, they ranged from 8 to 1 $m^2\ g^{-1}$ and were consistent with the electron microscopy images (S_{BET} increased with decreasing particle size). The size distribution histograms obtained from the TEM and SEM images are shown in Fig. 4. Most particles in sample S-800-0 had sizes from 40 to 70 nm, which fall in the nanometric range. Heating the spinel at 800 °C for 5 or 24 h resulted in more than 80% of particles having a size of 0.5–1 μm (i.e. in the submicro range). Sizes increased to 3–6 μm upon heating at 900 °C for 48 h. Crystallite size calculated from the Scherrer equation applied to the highest intensity XRD peak, Table 1, is consistent with the particle size obtained from electron microscopy images. Particles of sample S-900-48 are too big, line width too small and similar to instrumental broadening [30]. This introduces a significant error in the crystallite size values and the equation is unsuitable. In summary, by using an appropriate heating temperature and time, particles from nanometric to micrometric in size can be accurately obtained. The presence of the polymer increases the likelihood of obtaining a rather uniform particle size distribution in the nano-, submicro- and micro ranges.

3.2. Electrochemical characterization

The electrochemical response of the spinels was initially monitored by step potential electrochemical spectroscopy. Taking into account the similarity of S-800-5 and S-800-24 both in composition, cation distribution and particle size, we will describe the electrochemical properties of both samples in terms of the first. Fig. 5 shows the SPES curves for the three samples studied. As can be seen, the shape of curves for sample S-800-0 is consistent with a $LiNi_{0.5}Mn_{1.5}O_4$ spinel. The anodic scan exhibits two regions of electrochemical activity over the ranges 3.9–4.4 and 4.5–5.0 V, respectively. The main activity occurs in the 4.7–5.0 V region, the double peak in which is associated to the $Ni^{2+} \rightarrow Ni^{4+}$ process [31] (reportedly a cubic/cubic two-phase reaction [32]). The weak, broad peak at 4.1 V is related to the Mn^{3+}/Mn^{4+} redox couple. This suggests the presence of a small amount of Mn^{3+} the origin of which was assigned to NiO-based impurities [22]. Judging by their XRD patterns (see Fig. 1), our spinels seem to be free of impurities. One other plausible origin is the presence of some nickel ions as Ni^{3+}, as previously found by XPS [10,11]. On discharging the cell, the curve retains its features, but the peaks are shifted to somewhat lower potentials. Although the other two spinels continue to exhibit the two activity regions, the shape of curves is markedly different (see Fig. 5b and c). Thus, the area under the lower potential peak increases as the thermal treatment is intensified. This reflects an increase in Mn^{3+} content, which is consistent with the increase in unit cell dimension and the release of oxygen. Based on the peak area, the average oxidation state of Mn was 3.86 for S-800-5 and 3.77 for S-900-24. These values are closer to those determined from the stoichiometry as derived from the weight loss data (see Table 1). On the other hand, the peaks in the high-voltage region are broader and more ill-defined. In fact, the oxidation process goes beyond 5.0 V, which is the upper cutting voltage. This behavior is illustrative of the sluggish kinetics of lithium release and may be associated to an increased particle size or cation disorder, judging by the increased in the inverse spinel component. In fact, Talyosef et al. [33] found a similar behavior in microparticles but reported no structural data for the location of lithium. The shape of the discharge curves exhibited similar changes: an increase in the intensity of the lower voltage peak and an ill-defined, broad signal in the higher voltage region. On further cycling, splitting of the high-voltage peak was better resolved and revealed a faster kinetics for the electrochemical reaction. As shown below, this also reflected in the galvanostatic measurements.

The electrochemical performance of the three spinels (S-800-0, S-800-5 and S-900-48) was determined from galvanostatic measurements made over a wide range of charge/discharge rates (from *C*/4 to 4*C*) at cycling voltages from 3.5 to 5.0 V. In order to acquire a better understanding of the electrochemical behavior at high temperatures (50 °C), we extended measurements to room temperature (25 °C). Fig. 6a–c shows selected charge/discharge curves recorded at the latter temperature at *C*/4 in various cycles. The overall shape is consistent with that of SPES curves, with two pseudo-plateaux at *ca.* 4.0 and 4.6 V which can be assigned to the Mn^{3+}/Mn^{4+} and Ni^{2+}/Ni^{4+} redox couple, respectively. The best definition of these two regions of electrochemical activity with cycling was observed in the spinels S-800-0 and S-800-5, where, as with sample S-900-48, the discharge curve was strongly polarized in the first few cycles. The charge/discharge curves obtained on further cycling exhibited a shape consistent with the electrochemical behavior of the spinels. Fig. 7a–c shows the variation of the discharge capacity as a function of number of cycles. The results for the nanometric spinel S-800-0 were consistent with the expected behavior: a slight influence of the charge/discharge rate on the delivered capacity and good capacity retention on cycling. By contrast, the capacity delivered by spinel S-800-5 and, especially, S-900-48, was strongly dependent on the particular charge/discharge rate. The highest capacity was that for sample S-800-5 at *C*/4 and amounted to *ca.* 100 mAh g^{-1}, which is somewhat lower than the calculated value obtained on the assumption that all lithium was removed from tetrahedral positions (118 mAh g^{-1}). This is consistent with the fact that the charge/discharge curves largely retained their shape on cycling (see Fig. 6b). The capacity value decreased as current density increased. This was especially so for sample S-800-5 at 4*C* and for S-900-48 at both *C*/4 and 2*C*. The latter sample exhibited negligible capacity at 4*C*. The low capacity values obtained in the first cycle are consistent with the shape of the SPES (Fig. 5c) and charge/discharge curves (Fig. 6c), and reflect the sluggish kinetics of the electrochemical reaction by effect of the increased particle size and the resulting increase in the reaction path for removing and inserting lithium. Subsequently, the capacity gradually increases and eventually levels off on prolonged cycling. Under these conditions, the two pseudo-plateaux assigned to the redox reactions were clearly apparent. A somewhat different behavior was observed at 50 °C. Fig. 8a–c shows selected charge/discharge curves recorded at *C*/4 in various cycles. Under these conditions, only the curves for sample S-800-0 seemed strongly polarized after the first few cycles, with hardly any signs of lithium insertion/deinsertion (Fig. 8a). The curves for

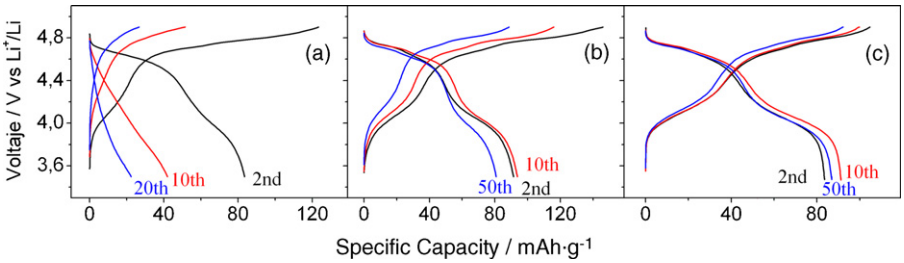

Fig. 8. Charge/discharge curves recorded at 50 °C at *C*/4 for samples (a) S-800-0, (b) S-800-5 and (c) S-900-48. The number of the cycles is shown.

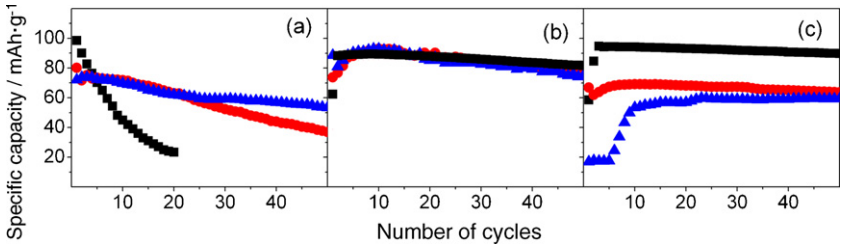

Fig. 9. Variation of specific capacity as a function of the number of cycles. Galvanostatic tests conducted at 50 °C. (a) S-800-0, (b) S-800-5 and (c) S-900-48. Rate: *C*/4 (black square); 2*C* (red circle); and 4*C* (blue triangle). (For interpretation of the references to color in this figure legend, the reader is referred to the web version of the article.)

the other two samples retained the pseudo-plateaux assigned to the two redox couples. In other words, the cell made from sample S-800-0 degraded faster than did those made from S-900-48. This can be more readily seen in Fig. 9a–c, where the capacity values are plotted against the number of cycles. As can be seen, the nanometric sample (Fig. 8a) exhibited an initial capacity of 100, 80 and 70 mAh g^{-1} at *C*/4, 2*C* and 4*C*, respectively; these values are comparable to those obtained at room temperature. However, the capacity faded on cycling, the decrease being especially pronounced at the lower charge/discharge rates, where a pronounced decrease in cell voltage was observed after the first few cycles (Fig. 8a). The decline in capacity retention can be associated with the diminished spinel stability under these conditions. It seems rather plausible that an increase in temperature may not only increase lithium mobility, but also increase the electrolyte reactivity, thereby also increasing the likelihood of active particles being attacked and dissolved by the electrolyte.

The micrometric sample S-900-48 behaved quite differently (see Fig. 6c). Thus, at *C*/4 it delivered a capacity of 95 mAh g^{-1} after the third cycle and retained most of it after 50 cycles. This can be ascribed to an increased stability of micrometric particles on prolonged contact with the electrolyte (e.g. at low rates). However, increasing the charge/discharge rate detracted from performance in the cell made from micrometric particles, particularly as regards the capacity delivered in the first few cycles (only 18 mAh g^{-1} at 4*C*). In any case, the temperature was clearly influential since the capacity measured at room temperature under this regime was negligible (see Fig. 5c). Similarly, the capacity tended to increase on further cycling, but the number of cycles needed was smaller at high temperatures, which is indicative of an increased lithium mobility. This was especially so at 4*C*, where the capacity in the 50th cycle was around 60 mAh g^{-1} and close to that obtained at 2*C*. In any case, these values are lower than those measured at *C*/4.

The increased capacity obtained on cycling at a high charge/discharge current density can be explained by assuming large particles to require a long enough time for the electrode–electrolyte interface to reach their inside. Once a certain portion of particles was accessible to the electrolyte, capacity retention was quite good. At high rates, however, the capacity was far from that calculated from the formula, which means that the portion of particles inaccessible to the electrolyte was still substantial. This suggests that the electrode–electrolyte interface was virtually immobilized once the soaking thickness became significant. The coating may act as a kinetic barrier hindering the electrode–electrolyte interface progress. With micrometric particles (4–6 μm in our case) lithium ions have to travel long distances and, only if the charge/discharge current densities are low, the interface can progress and considerably affect the particles. When the current density increases, the interface advance is slower than the electron flux supplied by the current and the delivered capacity is low. Under these conditions, several cycles are needed for the soaking layer to reach a certain thickness and hence the increased capacity observed. Reducing particle size, and hence the path length traveled by lithium, decreases the influence of the kinetic barrier and the capacity values and cycling properties conform to a more conventional pattern.

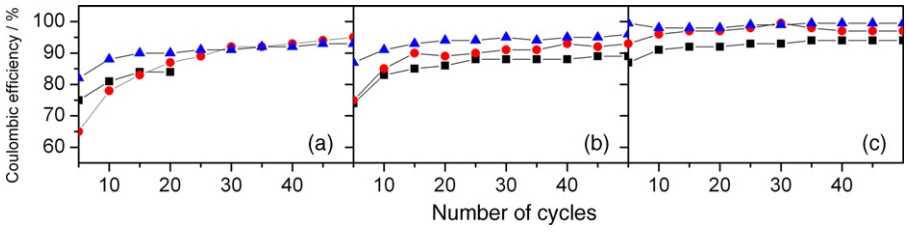

Fig. 10. Variation of the coulombic efficiency as a function of the number of cycles, at 50 °C, in samples (a) S-800-0, (b) S-800-5 and (c) S-900-48. Rate: *C*/4 (black square); 2*C* (red circle); and 4*C* (blue triangle). (For interpretation of the references to color in this figure legend, the reader is referred to the web version of the article.)

Sample S-800-5, which consisted of submicrometric particles, exhibited the best electrochemical performance at high temperatures (50 °C, Fig. 6b). The increased lithium-ion mobility was especially apparent at high rates, where the highest capacity was reached after the first few cycles. Seemingly, this spinel combines the strengths of nano and micrometric spinels. Thus, not only did it exhibit the good initial capacity typical of nanoparticles, but also it maintained the excellent capacity retention of the micrometric sample (Fig. 6c). The capacity values obtained after the first few cycles at the three rates were quite similar (around 90 mAh g^{-1}); also, capacity retention after 50 cycles was close to 90%.

One interesting inference from the previous results is the strong influence of particle size on the electrochemical activity of the spinel relative to other factors such as the presence of oxygen vacancies or the metal ion distribution in lattice positions. In fact, there is no clear relationship of such structural characteristics with electrochemical activity. Only particle size (nanometric, submicrometric or micrometric) thus seems to govern the electrochemical activity of the spinels. In this respect, it is somewhat surprising that spinels with a high Mn^{3+} content exhibit good electrochemical properties (particularly at high temperatures). The synthetic method used, which provides particles of appropriate uniform size and a high crystallinity, may account for the high stability of these spinels under such drastic experimental conditions.

Fig. 10 shows the coulombic efficiency of the three spinels cycled at 50 °C. As can be seen, it tended to approach 100% on cycling in all cases. However, there were some differences worth noting. Thus, the lowest values were obtained with the cells made from the S-800-0 spinel, which exhibited the worst cycling properties. The values for S-900-48 were somewhat higher than those for S-800-5 over the first ten cycles. However, the capacity delivered by the former spinel was quite low. Therefore, based on cell capacity, rate capability and coulombic efficiency, the spinel consisting of submicronic particles is the best for use as a cathode material in lithium cells.

4. Conclusions

Lithium-containing spinels are gaining interest in the field of Li ion batteries. $LiNi_{0.5}Mn_{1.5}O_4$ is one spinel with a promising future in this field, particularly for the production of a new generation of Li-ion batteries of higher energy. As shown in this work, the incorporation of a polymer (PMMA) into a simple synthetic method previously developed by our group [21] allows particle growth, and hence particle size, to be accurately controlled in order to ensure adequate battery performance. Electrochemical properties were examined over a wide range of charge/discharge rate (*C*/4, 2*C* and 4*C*) and at two different temperatures (room level and 50 °C). The latter temperature can easily be reached by large batteries such as those used in hybrid electric vehicles. At high temperatures, the best performance was obtained with the spinel prepared as particles of submicronic size. With this particle size, the spinel is quite stable against the attack of the electrolyte and maintains the retention capacity of micrometric particles at low charge/discharge rates. On the other hand, the path length for lithium-ion diffusion is shorter than with micrometric particles, which allows cells to respond to high rates. Other structurally related properties, such as cation arrangement or oxygen content seemingly have a minor influence.

Acknowledgements

This work was supported by CICYT (Project MAT2005-03069) and Junta de Andalucía (Group FQM 175).

References

[1] M. Winter, R.J. Brodd, Chem. Rev. 104 (2004) 4245.
[2] A.S. Aricó, P.G. Bruce, B. Scrosati, J.M. Tarascon, W. van Schalkwijk, Nat. Mater. 4 (2005) 366.
[3] G. Che, B.B. Lakshmi, E.R. Fisher, C.R. Martin, Nature 393 (1998) 346.
[4] Z. Zhang, A.J. Rondinone, J.X. Ma, J. Shen, S. Dai, Adv. Mater. 17 (2005) 1415.
[5] W.Y. Li, Li.N. Xu, J. Chen, Adv. Funct. Mater. 15 (2005) 851.
[6] J.C. Arrebola, A. Caballero, M. Cruz, L. Hernán, J. Morales, E. Rodríguez Castellón, Adv. Funct. Mater. 16 (2006) 1904.
[7] M.S. Whittingham, Chem. Rev. 104 (2004) 4271.
[8] C.G. Barlow, Electrochem. Solid State Lett. 2 (1999) 362.
[9] R. Benedek, M.M. Thackeray, Electrochem. Solid State Lett. 9 (2006) A265.
[10] K. Amine, H. Tukamoto, H. Yasuda, Y. Fujita, J. Electrochem. Soc. 143 (1996) 1607.
[11] A. Caballero, M. Cruz, L. Hernán, M. Melero, J. Morales, E. Rodríguez Castellón, J. Electrochem. Soc. 152 (2005) A552.
[12] Y. Talyosef, B. Markovsky, G. Salitra, D. Aurbach, H.J. Kim, S. Choi, J. Power Sources 146 (2005) 664.
[13] Y.K. Sun, Y.S. Lee, M. Yoshio, K. Amine, Electrochem. Solid State Lett. 5 (2002) A99.
[14] Z. Chen, J.R. Dahn, Electrochem. Solid State Lett. 6 (2003) A221.
[15] J.C. Arrebola, A. Caballero, M. Cruz, L. Hernán, J. Morales, E. Rodríguez Castellón, J.R. Ramos Barrado, J. Electrochem. Soc. 154 (2007) A178.
[16] R.Y. Hong, J.Z. Qian, J.X. Cao, Powder Technol. 163 (2006) 160.
[17] A. Jayaraman, G. Subramanyan, S. Shindu, P. Ajikumar, S. Valiyavettil, Cryst. Growth Des. 7 (2007) 142.
[18] M.M. Thackeray, S.D. Baker, K.T. Addendorf, J.B. Goodenough, Solid State Ionics 17 (1985) 175.
[19] B. Deng, H. Nakamura, M. Yoshio, Electrochem. Solid State Lett. 8 (2005) A171.
[20] A. Caballero, M. Cruz, L. Hernán, M. Melero, J. Morales, E. Rodríguez Castellón, J. Power Sources 150 (2005) 192.
[21] J.C. Arrebola, A. Caballero, L. Hernán, M. Melero, J. Morales, E. Rodríguez Castellón, J. Power Sources 162 (2006) 606.
[22] Y. Ein-Eli, J.T. Vaughey, M.M. Thackeray, S. Mukerjee, X.Q. Yang, J. McBreen, J. Electrochem. Soc. 146 (1999) 908.
[23] M. Kunduraci, G.G. Amatucci, J. Electrochem. Soc. 153 (2006) A1345.
[24] Y. Takahashi, H. Sasaoka, R. Kuzuo, N. Kijima, J. Akimoto, Electrochem. Solid State Lett. 9 (2006) A203.
[25] Y.S. Lee, Y.K. Sun, S. Ota, T. Miyashita, M. Yoshio, Electrochem. Commun. 4 (2002) 989.
[26] Y. Kobayashi, H. Miyashiro, K. Takei, H. Shigemura, M. Tabuchi, H. Kageyama, T. Iwahori, J. Electrochem. Soc. 150 (2003) A1577.
[27] A. Caballero, L. Hernán, M. Melero, J. Morales, M. Angulo, J. Electrochem. Soc. 152 (2005) A6.
[28] A.C. Larson, R.B. Von Dreele, Los Alamos National Lab. Rep. No. LA-UR-86-748, 1994.
[29] Y. Wong, M.G. Kim, Y. Kim, Y. Lee, J. Cho, Electrochem. Solid State Lett. 9 (2006) A34.
[30] J. Morales, J.L. Tirado, M. Macias, J. Solid State Chem. 53 (1984) 303.
[31] Y. Terada, Y.K. Masaka, F. Nishikawa, T. Konishi, M. Yoshio, I. Nakai, J. Solid State Chem. 156 (2001) 286.
[32] K. Ariyoshi, Y. Iwakoshi, N. Nakayama, T. Ohzuku, J. Electrochem. Soc. 151 (2004) 296.
[33] Y. Talyosef, B. Marskovski, R. Lavi, G. Salitra, D. Aurbach, D. Kovacheva, M. Gorova, E. Zhecheva, R. Stoyanova, J. Electrochem. Soc. 154 (2007) A682.